PHYSICAL REVIEW C VOLUME 41, NUMBER 4 APRIL 1990

# Transverse momenta, nuclear equation of state, and momentum-dependent interactions in heavy-ion collisions

C. Gale,[a] G. M. Welke,[b] M. Prakash,[b] S. J. Lee,[a],* and S. Das Gupta[a]
[a] *Physics Department, McGill University, Montréal, Québec, Canada H3A 2T8*
[b] *Physics Department, State University of New York at Stony Brook, Stony Brook, New York 11794*
(Received 5 May 1989)

We investigate the generation of transverse momentum in high-energy heavy-ion collisions and its relation to the nuclear equation of state. We find that streamer chamber data can be fitted by Boltzmann-Uehling-Uhlenbeck calculations with a momentum-dependent potential that closely models realistic nuclear matter interactions and yields an equation of state with $K=215$ MeV.

## I. INTRODUCTION

Extracting information about the nuclear equation of state (EOS) has been a major goal of intermediate-energy heavy-ion collisions. Of the several observables suggested to obtain limits on the nuclear compressibility, measurements of transverse momenta[1,2] have raised much optimism. Other complementary observables are flow angles,[3] azimuthal distributions about the reaction plane,[4] etc. It is hoped that mass transport properties can be directly related to the nuclear EOS.

In this paper we address the issue of magnitudes of transverse momenta and their relationship to any particular mean field used in Boltzmann-Uehling-Uhlenbeck (BUU) calculations.[5] By considering simple mean fields without momentum dependence and also a more realistic mean field with momentum dependence, we study the relationship between the mean field and the amount of transverse momenta generated. Such relationships are not simple and direct as one might *a priori* expect as the behavior of large amplitude motion in Vlasov dynamics is quite different than in other forms of matter.

The plane of the paper is as follows. In Sec. II we briefly describe the simple mean fields to be used in BUU calculations. Here we also make comparisons with realistic nuclear matter calculations that have been performed recently. In Sec. III we investigate the role of the mean field in the generation of transverse momenta. Related mathematical details are given in the Appendix. In Sec. IV results of our calculations are compared with some recent experimental data. Conclusions are presented in Sec. V.

## II. MEAN-FIELD PARAMETRIZATIONS

The simplest mean-field parametrization is obtained when the potential energy density $V$ and the one-body potential $U$ are functions of density alone. We choose the forms used by Bertsch, Kruse, and Das Gupta (BKD),[6] viz.

$$V(\rho)=\frac{A}{2}\frac{\rho^2}{\rho_0}+\frac{B}{\sigma+1}\frac{\rho^{\sigma+1}}{\rho_0^{\sigma}} , \tag{2.1}$$

$$U(\rho)=A\left[\frac{\rho}{\rho_0}\right]+B\left[\frac{\rho}{\rho_0}\right]^{\sigma} . \tag{2.2}$$

The constants $A$, $B$, and $\sigma$ are chosen to reproduce the known binding energy $E/A$, the saturation density $\rho_0$, and a guessed compression modulus $K$. We use two sets of parameters: (1) $A=-356$ MeV, $B=303$ MeV, and $\sigma=\frac{7}{6}$, which give $K=200$ MeV. We call this parametrization soft BKD (SBKD). (2) $A=-124$ MeV, $B=70.5$ MeV, and $\sigma=2$, which give $K=380$ MeV. This parametrization is termed hard BKD (HBKD).

A more realistic parametrization should account for the fact that the one-body potential must also be a function of the momentum $\mathbf{p}$ that a nucleon has with respect to the medium. The evidence comes from the experimental behavior of the real part of the optical potential. Welke *et al.*[4] used the parametrization

$$V(\rho)=\frac{A}{2}\frac{\rho^2}{\rho_0}+\frac{B}{\sigma+1}\frac{\rho^{\sigma+1}}{\rho_0^{\sigma}}+\frac{C}{\rho_0}\int\int d^3p\, d^3p'\frac{f(\mathbf{r},\mathbf{p})f(\mathbf{r},\mathbf{p}')}{1+\left[\frac{\mathbf{p}-\mathbf{p}'}{\Lambda}\right]^2} , \tag{2.3}$$

which leads to a potential

$$U(\rho,\mathbf{p})=A\left[\frac{\rho}{\rho_0}\right]+B\left[\frac{\rho}{\rho_0}\right]^{\sigma}+2\frac{C}{\rho_0}\int d^3p'\frac{f(\mathbf{r},\mathbf{p}')}{1+\left[\frac{\mathbf{p}-\mathbf{p}'}{\Lambda}\right]^2} . \tag{2.4}$$

Here $f(\mathbf{r},\mathbf{p})$ is the phase-space density; the configuration space density $\rho(\mathbf{r})=\int f(\mathbf{r},\mathbf{p})d^3p$. There are five constants in Eqs. (2.3) and (2.4); these are found by requiring that $E/A=-16$ MeV, $\rho_0=0.16$ fm$^{-3}$, $K=215$ MeV, $U(\rho_0,p=0)=-75$ MeV, and $U(\rho_0,p^2/(2m)=300\text{ MeV})=0$. Their values are then $A=-110.44$ MeV, $B=140.9$ MeV, $C=-64.95$ MeV, $\sigma=1.24$, and $\Lambda=1.58\, p_F^{(0)}$, and yield an effective mass $m^*=0.67\, m$ at the Fermi surface. With these parameters the potential in cold nuclear matter becomes repulsive for energy greater than 300 MeV reaching an asymptotic value of 30.5 MeV. The momentum dependence in Eq. (2.4) arises from the exchange term of a Yukawa force. We therefore refer to this interaction as a momentum-dependent Yukawa interaction (MDYI).

A simpler version of Eq. (2.3) was used by Gale, Bertsch, and Das Gupta (GBD) (Ref. 7), where for simplicity an averaging was done for one of the integrals in Eq. (2.3). This gives

$$V(\rho)=\frac{A}{2}\frac{\rho^2}{\rho_0}+\frac{B}{\sigma+1}\frac{\rho^{\sigma+1}}{\rho_0^{\sigma}}+\frac{C_\rho}{\rho_0}\int d^3p\frac{f(\mathbf{r},\mathbf{p})}{1+\left[\frac{\mathbf{p}-\langle\mathbf{p}\rangle}{\Lambda}\right]^2}, \tag{2.5}$$

which leads to

$$U(\rho,\mathbf{p})=A\left[\frac{\rho}{\rho_0}\right]+B\left[\frac{\rho}{\rho_0}\right]^{\sigma}+\frac{C}{\rho_0}\int d^3p'\frac{f(\mathbf{r},\mathbf{p}')}{1+\left[\frac{\mathbf{p}'-\langle\mathbf{p}'\rangle}{\Lambda}\right]^2}+\frac{C}{\rho_0}\frac{\rho}{1+\left[\frac{\mathbf{p}-\langle\mathbf{p}\rangle}{\Lambda}\right]^2}. \tag{2.6}$$

The parameters chosen were $A=-144$ MeV, $B=203.3$ MeV, $C=-75$ MeV, $\sigma=\frac{7}{6}$, and $\Lambda=1.5\,p_F^{(0)}$. We will refer to this parametrization as the GBD interaction.

Other authors[8,9] have also used momentum-dependent interactions, although not within the framework of the BUU formalism.

Of the four mean-field parametrizations just given, MDYI is the most realistic. In Sec. IV we will use this in BUU calculations to compare with experimental data. It is therefore pertinent to enquire if results of more microscopic calculations are reproduced by MDYI. Wiringa[10] has calculated the single-particle potential in nuclear matter using several realistic Hamiltonians for densities ranging from 0.1 to 0.5 fm$^{-3}$. These Hamiltonians include nucleon-nucleon potentials fit to scattering data and three nucleon potentials fit to binding energies of few-body nuclei and saturation properties of nuclear matter. The results of these microscopic calculations were parametrized and the values of the parameters are given in Table I of Ref. 10. We use this table to compare Wiringa's calculations with $U(\rho,\mathbf{p})$ obtained from MDYI [Eq. (2.4)] Comparisons with results of UV14+TNI (see Fig. 1) and UV14+UVII (see Fig. 2) interactions show that $U(\rho,\mathbf{p})$ obtained from MDYI is very reasonable. In Fig. 1 better agreement could be obtained by a small increase in the compression modulus in MDYI, but such fine tuning is not warranted for our purposes. For completeness we also show a comparison of $U(\rho,\mathbf{p})$ from GBD with UV14+TNI in Fig. 3. The agreement is not as good as with MDYI but, of course, still far superior to

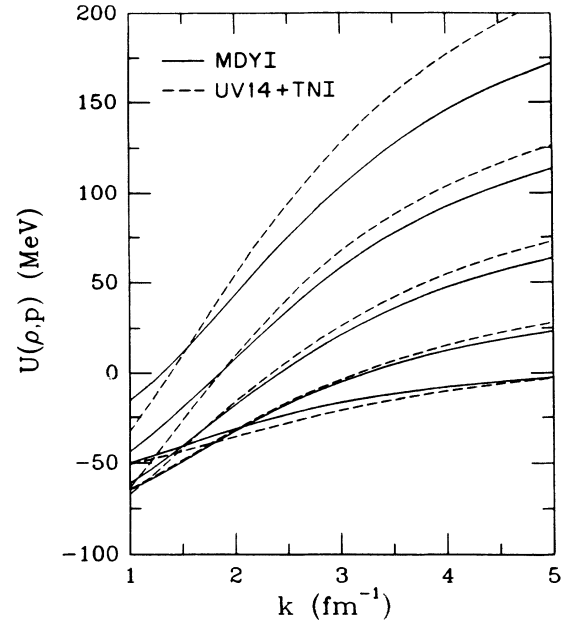

FIG. 1. A comparison of the single-particle potential from MDYI [Eq. (2.4)] with the microscopic calculations of Wiringa (Ref. 10) using the UV14+TNI interaction. The abscissa shows wave numbers. Starting from the bottom at right, the different curves are for densities of 0.1, 0.2, 0.3, 0.4, and 0.5 fm$^{-3}$.

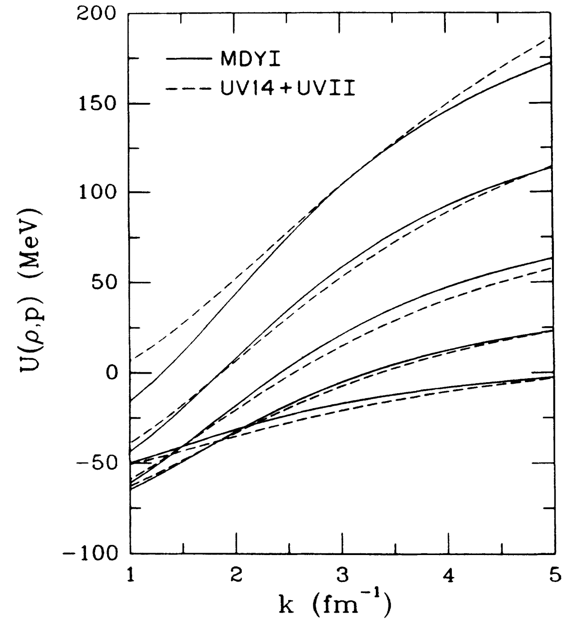

FIG. 2. A comparison of the single-particle potential from MDYI [Eq. (2.4)] with the microscopic calculations of Wiringa (Ref. 10) using the UV14+UVII interaction. The abscissa shows wave numbers. Starting from the bottom at right, the different curves are for densities of 0.1, 0.2, 0.3, 0.4, and 0.5 fm$^{-3}$.

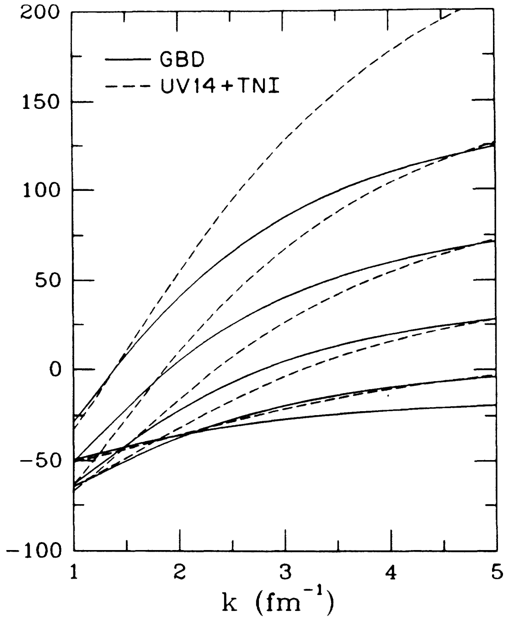

FIG. 3. A comparison of the single-particle potential from GBD [Eq. (2.6)] with the microscopic calculations of Wiringa (Ref. 10) using the UV14+TNI interaction. The abscissa shows wave numbers. Starting from the bottom at right, the different curves are for densities of 0.1, 0.2, 0.3, 0.4, and 0.5 fm$^{-3}$.

what one would get with SBKD or HBKD.

The preceding results show that a BUU calculation based on MDYI has much to recommend, as MDYI provides a good representation of $U(\rho,\mathbf{p})$ at zero temperature for a wide range of density and momentum. The specific form of momentum dependence is easily seen to emerge from the exchange term of a Yukawa force in nuclear matter or equivalently in the local density limit. It can be expected to exhibit proper behavior under a broad range of conditions.

## III. TRANSVERSE MOMENTA AND EQUATIONS OF STATE

It has been known for some time that a momentum-dependent interaction that yields a soft equation of state can provide about the same transverse momenta as a hard BKD.[4,7,9] If we combine this observation with the expectation that transverse momenta reflect the properties of EOS's we will be tempted to conclude that the EOS's based on both these interactions become similar for high temperatures ~60 MeV. We shall follow this line of thought for the present and construct finite temperature EOS's for the various interactions.

Equation of state curves are traditionally plots of pressure $P$ vs density $\rho$ for constant temperature $k_BT=1/\beta$. We will compare such curves for HBKD, SBKD, MDYI, and GBD. It suffices to show how such curves are calculated for MDYI, since this is the most involved. For thermal equilibrium, the starting point of such a calculation requires finding the occupation probability

$$n[\epsilon(p)]=\frac{1}{e^{\beta[\epsilon(p)-\mu]}+1} \tag{3.1}$$

for a given temperature $1/\beta$ and density $\rho$. If $\epsilon(p)$ was known *a priori* this would merely entail finding the chemical potential $\mu$ from the equation

$$\rho=\frac{16\pi}{h^3}\int_0^\infty dp\, p^2 n[\epsilon(p)] \ . \tag{3.2}$$

However, for MDYI, the expression for $\epsilon(p)$ is [the potential part is from Eq. (2.4)]

$$\epsilon(p)=\frac{p^2}{2m}+A\left[\frac{\rho}{\rho_0}\right]+B\left[\frac{\rho}{\rho_0}\right]^\sigma+R(\rho,p)\ , \tag{3.3}$$

where at finite temperature

$$R(\rho,p)=2\frac{C}{\rho_0}\frac{4}{h^3}\int d^3p'\frac{1}{e^{\beta[\epsilon(p')-\mu]}+1}\times\frac{1}{1+\left[\frac{\mathbf{p}-\mathbf{p}'}{\Lambda}\right]^2} \ . \tag{3.4}$$

Thus knowing $R(\rho,p)$ requires knowing $R(\rho,p')$ for all values of $p'$. There is therefore a self-consistency condition to be fulfilled just as in Hartree-Fock theory.

Fortunately this self-consistency problem is readily solved by the following iterative scheme. Make an initial guess for $R(\rho,p)$ from the zero-temperature condition

$$R^{(0)}(\rho,p)=2\frac{C}{\rho_0}\frac{4}{h^3}\int d^3p'\frac{1}{1+\left[\frac{\mathbf{p}-\mathbf{p}'}{\Lambda}\right]^2}\ , \tag{3.5}$$

where $\rho=(16\pi/3h^3)p_F^3$. This is then used in Eqs. (3.1) and (3.2) with the desired temperature to obtain $\mu^{(0)}$. With this $\epsilon^{(0)}(p)$ and $\mu^{(0)}$ we now obtain $R^{(1)}(\rho,p)$ from Eq. (3.4). This in turn gives $\epsilon^{(1)}(p)$, which is used in Eqs. (3.1) and (3.2) to find $\mu^{(1)}$. The cycle is repeated and a few iterations suffice to achieve convergence.

With known values of $n[\epsilon(p)]$ the pressure can be computed. In Appendix E of Ref. 5 an expression for the pressure tensor is given that is general and does not assume equilibrium [equilibrium here means that $n[\epsilon(p)]$ is given by the Fermi occupation factor Eq. (3.1)]. This expression is

$$P_{ij}=\int d^3p\, p_i\left[\frac{p_j}{m}+\nabla_p^j U\right]f+\delta_{ij}\left[\int d^3p\, Uf-V\right]\ . \tag{3.6}$$

In equilibrium Eq. (3.6) gives $P_{ij}=\delta_{ij}P$ and $P$ will give the same answer as the more well-known procedure of calculating pressure. This equivalence is demonstrated in the Appendix. Starting with the grand potential

$$\Omega=E-TS-\mu N\ , \tag{3.7}$$

thermodynamics gives

$$\left[\frac{\partial\Omega}{\partial\mathcal{V}}\right]_{\mu,T}=-P\ . \tag{3.8}$$

For $\mu, T$ fixed, $E$, $S$, and $N$ depend linearly on volume $\mathcal{V}$; thus one may equivalently use $(-\Omega/\mathcal{V})=P$). Thus we calculate

$$P=a+b+c \ , \tag{3.9}$$

$$a=-V-\frac{16\pi}{h^3}\int_0^\infty dp\frac{p^4}{2m}n[\epsilon(p)] \ , \tag{3.10}$$

where $V$ is given by Eq. (2.3) and

$$b=-\frac{1}{\beta}\frac{16\pi}{h^3}\int_0^\infty dp\, p^2[n\ \ln n+(1-n)\ln(1-n)] \ , \tag{3.11}$$

$$c=\mu\frac{16\pi}{h^3}\int_0^\infty dp\, p^2 n[\epsilon(p)]=\mu\rho \ . \tag{3.12}$$

The EOS's obtained with SBKD, HBKD, MDYI, and GBD are shown in Fig. 4, where we have used temperatures of 40 and 80 MeV. Note that SBKD, GBD, and MDYI curves are quite close to each other; HBKD stands apart from the others even at temperature as high as 80 MeV. It is, however, well known that HBKD and a momentum-dependent interactions can generate about the same transverse momenta,[4,7,9] and that SBKD produces less. We thus come to the conclusion (a) two EOS's (HBKD and MDYI) that are rather dissimilar over a wide range of temperatures can produce similar transverse momenta and (b) two EOS's (SBKD and MDYI) that are similar can produce different transverse momenta.

In an effort to understand this we plot in Fig. 5 the growth of transverse momenta as a function of time obtained from BUU calculations. A good fraction of the final average transverse momenta is generated quite early in the history of the "hit." At this point, a sufficient number of hard collisions have not yet taken place to achieve thermal equilibrium. Thus the values of pressure at fixed temperatures are not very relevant. An exactly opposite idealization may be more pertinent for the computation of pressure relevant for transverse momentum production. Consider nuclear matter at density $\rho$; half the nucleons with their associated Fermi momenta move with mean momentum $p_0\hat{z}$, the other half with their associated Fermi momenta move with mean momentum $-p_0\hat{z}$. For 400- and 800-MeV/nucleon beam energies, the values of $p_0$ are such that the two Fermi spheres are disjoint in momentum space, although there is complete overlap in configuration space. Such a scenario was considered in Ref. 4. The pressure in this situation can be computed from Eq. (3.6). For momentum-dependent interactions this is more complicated than for momentum-independent interactions; we therefore provide some details in the Appendix.

Figure 6 compares the pressure in this idealized situation for various interactions. At 400-MeV beam energy GBD produces more pressure than HBKD up to density $1.6\rho_0$; at 800 MeV it produces more pressure than HBKD up to $2\rho_0$. The figure allows us to qualitatively understand why both GBD and HBKD can produce similar transverse momenta. However from Fig. 6, it is not at all obvious why MDYI also produces similar transverse momenta as HBKD. The reason this happens is quite intri-

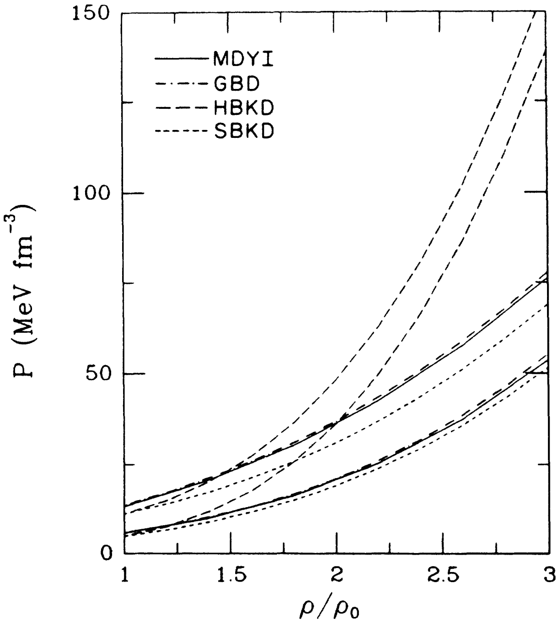

FIG. 4. Equilibrium pressure versus density in units of the equilibrium density 0.16 fm$^3$ for the MDYI, GBD, HBKD, and SBKD interactions. For each curve designation, the lower (upper) curve corresponds to a temperature of $T=40(80)$ MeV.

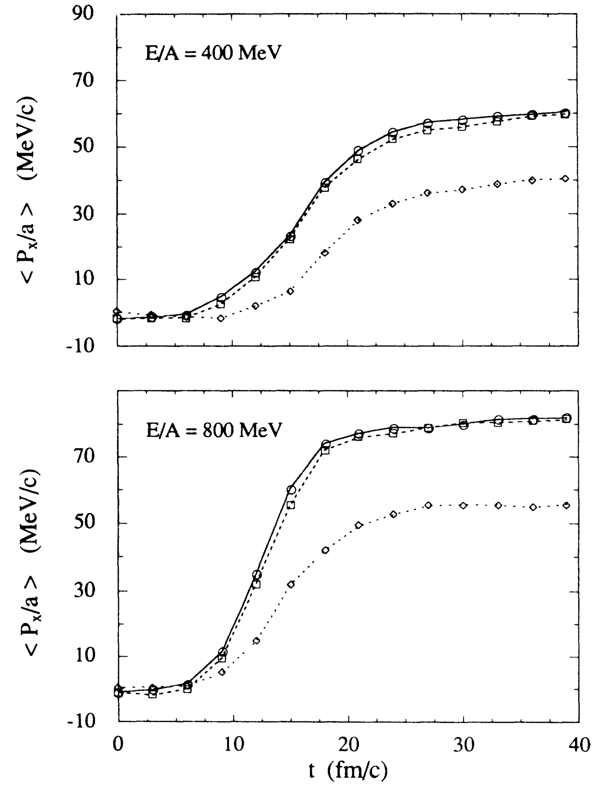

FIG. 5. Average transverse momenta versus time from BUU calculations for La+La at an impact parameter $b=2.67$ fm. Results from MDYI (solid curves), HBKD (long-dashed curves) and SBKD (short-dashed curves) are shown.

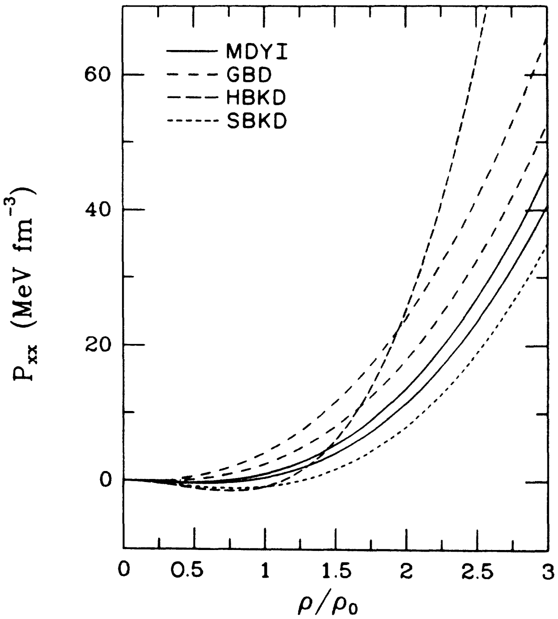

FIG. 6. The pressure tensor element transverse to the beam axis for the HBKD, SBKD, GBD, and MDYI potentials as a function of density. For the MDYI and GBD interactions, the lower (upper) curves correspond to $E/A = 400(800)$ MeV.

guing and is given in the following.

Both mean field and hard collisions cooperate in producing transverse momenta and both are important, but, in an effort to understand what the mean field by itself can do we will switch off hard collisions. Figure 7 shows the results from a pure Vlasov calculation with SBKD, HBKD, and MDYI. We see that SBKD produces small negative transverse momenta and HBKD produces small positive transverse momenta, whereas MDYI produces significant positive transverse momenta.

It is desirable to have a simple understanding of these results. Heavy-ion collisions in Vlasov dynamics can be quite complicated but the main features of these results can be understood in a simple model suggested by G. F. Bertsch.[11] At 800 MeV/nucleon the two nuclei basically pass through each other in the mean-field approximation. Let us make an even simpler approximation that at this energy the phase-space distribution of each nucleus remains unaltered, at all times during the collision, except for possible center-of-mass shifts in configuration and momentum space. The problem is then equivalent to the scattering of two particles with the Hamiltonian

$$H=(E_K)_1+(E_K)_2+[\tilde{V}(R)-\tilde{V}(2R_0)]\ , \tag{3.13}$$

where $\tilde{V}(R)$ is the potential energy when the centers of the two ions are separated by a distance $R$. For $R$ less than $2R_0$ ($R_0$ is the radius of each nucleus) this potential follows from geometry,

$$\tilde{V}(R)=\left[\frac{4\pi}{3}R_0^3-\pi R_0^2 R+\frac{\pi}{12}R^3\right]V(2\rho_0)+\left[2\pi R_0^2 R-\frac{\pi}{6}R^3\right]V(\rho_0)\ . \tag{3.14}$$

For $R>2R_0$, we have $\tilde{V}(R)=\tilde{V}(2R_0)=V(\rho_0)8\pi/3R_0^3$. For SBKD and HBKD, $V(2\rho_0)$ and $V(\rho_0)$ are calculated from Eq. (2.1). For MDYI, they can be computed using Eqs. (2.3) and (A4). The resulting expression contains terms that depend upon the relative momentum of the two colliding ions, which for the purpose of calculating $V(2\rho_0)$ was kept fixed at the original value. The error of this approximation is small. We have thus replaced the problem of scattering of two heavy ions in the mean-field approximation to that of scattering of two objects by a potential

$$\tilde{V}(R)-\tilde{V}(2R_0)=\frac{4\pi R_0^3}{3}[V(2\rho_0)-2V(\rho_0)]\times\left[1-\frac{3}{2}\left[\frac{R}{2R_0}\right]+\frac{1}{2}\left[\frac{R}{2R_0}\right]^3\right]\ , \tag{3.15}$$

which is shown in Fig. 8. This figure suggests that the

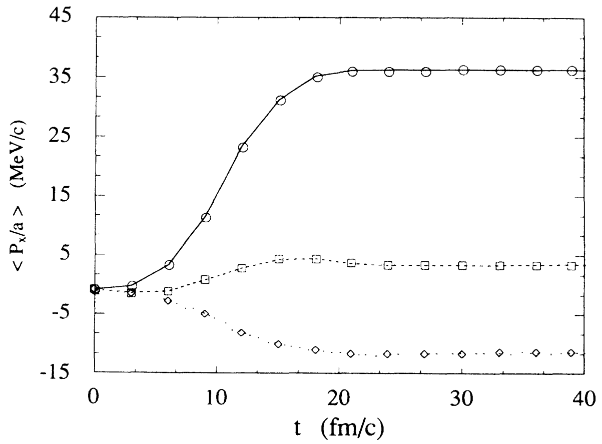

FIG. 7. Average transverse momenta versus time from Vlasov calculations for La+La at an impact parameter $b = 2.67$ fm. Results from MDYI, HBKD, and SBKD are shown by solid, long-dashed and short-dashed curves, respectively.

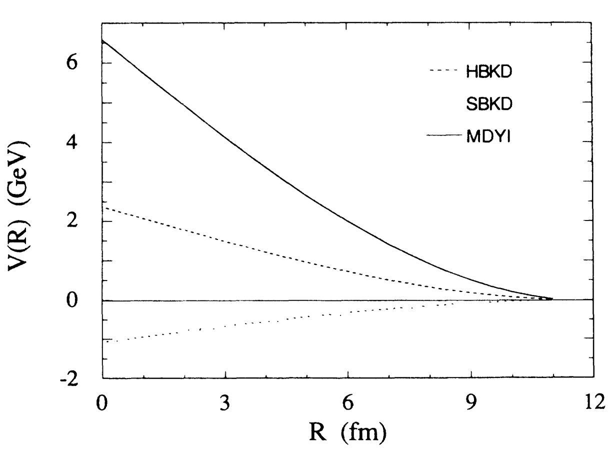

FIG. 8. The potential in Eq. (3.13) as a function of the separation distance $R$ of two La nuclei for the MDYI, HBKD, and SBKD interactions. The curves correspond to $E/A = 800$ MeV.

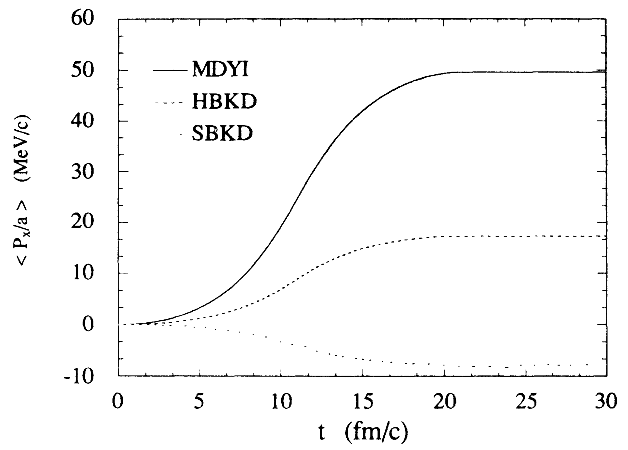

FIG. 9. The transverse momentum per nucleon for the two-body scattering problem using Eqs. (3.13) and (3.14). The curves correspond to $E/A = 800$ MeV and the impact parameter $b = 2.67$ fm as in Fig. 7.

transverse momentum will be small and negative for SBKD, small and positive for HBKD, and large and positive for MDYI. Solving the scattering problem using Eqs. (3.13) and (3.14), the transverse momenta generated are shown in Fig. 9. The similarity of these results to those in Fig. 7 suggests that this simple model incorporates much of the physics of Vlasov dynamics at this energy.

One can now understand why in a full calculation including both Vlasov and hard collisions the transverse momenta generated by MDYI and HBKD can be similar. In mean-field propagation, MDYI produces more transverse momentum than HBKD. Two-body collisions tend to equilibrate the participants, and in complete equilibrium, HBKD produces more transverse momentum. The combination of these two mechanisms for producing transverse momentum therefore yields similar results for HBKD and MDYI.

## IV. COMPARISONS WITH DATA

In this section we compare our BUU calculations with experimental data. We have chosen to focus on one particular set of experiments performed using the Streamer Chamber facility at the Bevalac.[12] Accordingly, we present results for near central reactions of Ar+KCl, La+La, and Ar+Pb at 800 MeV/nucleon. We have analyzed the final state of our numerical simulations in terms of the transverse momentum[1] and sphericity tensor techniques.[13] The maximum impact parameter was evaluated in each case by fitting the experimental trigger cross section with a geometrical clean-cut model, as prescribed in Ref. 12. For the case of Ar+KCl, where the data set consisted of unbiased samples of events from two different reactions, the integrations over impact parameter were appropriately weighted before being combined. The values of $b_{\max}$ used were 2.4 and 5.3 fm for Ar+KCL, 5.5 fm for Ar+Pb, and 8.5 fm for La+La. As usual, the calculations of many nuclear collisions were performed in parallel to obtain meaningful statistics and to minimize numerical fluctuations in the nuclear mean field. The number of runs was 120, 60, and 50 for Ar+KCl, Ar+Pb and La+La, respectively. The inputs to the BUU simulation are the interaction specified by Eq. (2.4) and free space nucleon-nucleon scattering cross sections.[5] In this respect, note that the propagation and scattering of test particles in a momentum-dependent mean field deserve some care. Several complications arise, owing to the nonlocality of the interaction. If the mean field were momentum independent then in collisions between test particles both the total momentum and the magnitude of the relative momentum should be constant (for elastic scattering). This prescription introduces some energy nonconservation when the mean field is momentum dependent. This has been ignored in previous calculations[4,5,7] and, for most parts, in the results reported here. A detailed investigation of this effect as well as other possible in-medium modifications[14-17] of the nuclear transport coefficients will be published later. We have verified that the energy nonconservation, while not too large, is not entirely negligible. We are presently developing an iterative scheme for this correction. For the purpose of the present work we have used a first order correction rather than the full iteration. Doing this, we observe that energy conservation is improved but no

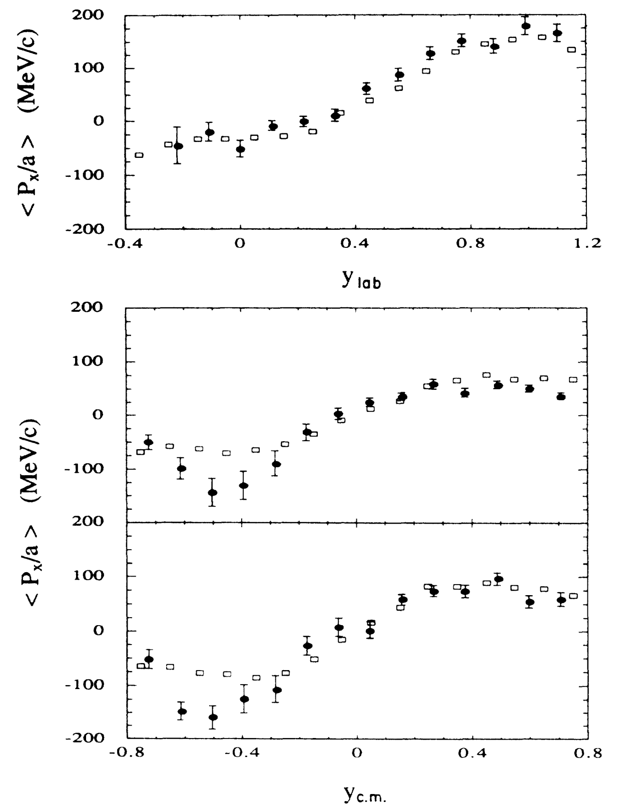

FIG. 10. Transverse momentum per nucleon as a function of rapidity in reactions of 800 MeV per projectile nucleon. Results of BUU simulations with the MDYI interaction (open squares) are compared with the data of Ref. 12 (solid circles). Results for Ar+Pb are in the lab, for La+La and Ar+KCl in the center of mass.

TABLE I. We compare the values obtained with our BUU approach with the experimental data of Ref. 12, for symmetric systems. We estimate the numerical uncertainties to be $\approx \pm 2$ MeV/$c$ for the transverse momentum results and $\approx \pm 0.5$ deg for the flow angles.

| System | $(\theta_f)^{\text{This work}}$ (deg) | $(\theta_f)^{\text{Expt.}}$ (deg) | $\langle p_x \rangle^{\text{This work}}_{y>0.15}$ (MeV/$c$) | $\langle p_x \rangle^{\text{Expt}}_{y>0.15}$ (MeV/$c$) |
|---|---|---|---|---|
| Ar+KCl | 12 | 9.6±0.8 | 61 | 50±4 |
| La+La | 11 | 16.5±1.7 | 76 | 72±6 |

significant changes in the values of transverse momenta, flow angle, etc. were found.

Let us first consider the transverse momentum results. We calculate the average momentum per nucleon in the true reaction plane, for each rapidity interval. For the symmetric Ar+KCl and La+La reactions, we plot this in the center of mass of the colliding nuclei. For the case Ar+Pb, we chose to bypass the difficulties associated with center-of-mass determination and used the laboratory data instead. Note that the data consists of deuterons only but the authors of Ref. 12 report that their measurements and detector efficiency simulations are consistent with deuteron momenta being twice those of protons in a given rapidity interval. We can therefore compare with our BUU final states that contain almost exclusively nucleons. We have further imposed a "spectator cut" by leaving out particles that had undergone no collisions from the analysis.

Our results are shown in Fig. 10 together with the data from Ref. 12. Because of particle detection inefficiencies, the experimental transverse momenta in the backward direction are artificially biased towards large negative values and are therefore unreliable. Concentrating on the forward direction, we see that the overall agreement is quite remarkable. In all cases, the experimental maximum transverse momentum and the slope near the rapidity origin are reproduced by our calculations. The maximum transverse momentum generated by the reaction Ar+Pb is the largest reported so far in the literature. Our calculations with MDYI reproduce this data quite well.

The sphericity analysis was performed by diagonalizing the tensor

$$P_{ij} = \sum_{\mu} \frac{p_i(\mu) p_j(\mu)}{|\mathbf{p}|} , \tag{4.1}$$

where $p_i$ is a cartesian momentum coordinate. The sum runs through all events contributing to a given reaction cross section and over all baryons detected in the forward hemisphere. We then obtain a flow angle, in the usual fashion, for Ar+KCl and La+La. Once again we did not search for the Ar+Pb center of mass on an event by event basis and therefore a value for $\theta_f$ is not quoted. The calculated flow angles and the transverse momenta averaged over a region such that $y_{\text{c.m.}} > 0.15$ are shown in Table I and are seen to be in good agreement with the experimental values. We must, however, note that these numbers are quite sensitive to the precise multiplicity-impact parameter mapping. Such is not the case for the transverse momentum versus rapidity plots.

Summarizing this section, we obtain good overall agreement between the Streamer Chamber data and BUU calculations using a momentum-dependent mean field. This single-particle potential yields a soft equation of state with $K = 215$ MeV.

## V. CONCLUSIONS

The momentum-dependent single-particle potential $U(\rho, \mathbf{p})$ used in this work (MDYI) is in quantitative agreement with realistic nuclear matter calculations and also reproduces the optical potential data. We therefore believe such a force to be appropriate for numerical simulations of heavy-ion collisions over a wide range of energies. This mean field yields a nuclear matter incompressibility of 215 MeV.

BUU calculations using this mean field reproduce the transverse momentum and flow angle data from the Streamer Chamber. A sizable fraction of the flow is determined in the early phases of the reaction, where equilibrium cannot possibly exist. It is, in fact, sensitive to the initial-state correlation, which the momentum dependence of the interaction would tend to preserve.

Therefore an important consequence of our study is that the transverse momentum analysis at intermediate energies is not a *direct* probe of the nuclear equation of state, as previously thought. A corollary is that only models that start from a nonequilibrium initial state, and include both a realistic momentum-dependent interaction and a relaxation mechanism, are pertinent to the study of heavy-ion collisions in the energy range discussed here.

## ACKNOWLEDGMENTS

We acknowledge many discussions with G. F. Bertsch and P. Danielewicz throughout this investigation and we thank the latter for the experimental data in tabular form. G. E. Brown provided much impetus for this study. We further acknowledge the Cyber 990 computer facilities at the Chalk River Nuclear Laboratories. This work was supported in part by the Department of Energy under Grant No. DE-FG02-88ER40388, in part by the Natural Sciences and Engineering Research Council of Canada, and in part by the Québec Department of Education.

## APPENDIX

### 1. Equilibrium Pressure

In equilibrium $P_{ij} = \delta_{ij} P$ and the expression for $P$ from Eq. (3.6) becomes

$$P=P_{xx}=\frac{4}{h^3}\int d^3p\left[\frac{p_x^2}{m}+p_x\frac{\partial U}{\partial p_x}\right]n[\epsilon(p)]+A\frac{\rho^2}{\rho_0}+B\frac{\rho^{\sigma+1}}{\rho_0^\sigma}+\frac{16\pi}{h^3}\int dp\,p^2R(\rho,p)n[\epsilon(p)]-V\;, \tag{A1}$$

where $V$ is given by Eq. (2.3). This reduces to

$$\begin{aligned}P=P_{xx}=&\frac{16\pi}{h^3}\int dp\left[\frac{p^4}{3m}+\frac{p^3}{3}\frac{\partial U}{\partial p}\right]n(\epsilon(p))+\frac{A}{2}\frac{\rho^2}{\rho_0}+B\frac{\sigma}{\sigma+1}\frac{\rho^{\sigma+1}}{\rho_0^\sigma}\\&+\frac{16\pi}{h^3}\int dp\,p^2R(\rho,p)n[\epsilon(p)]-\left[\frac{4}{h^3}\right]^2\frac{C}{\rho_0}\int d^3p\,d^3p'\frac{n(p)n(p')}{1+\left[\frac{\mathbf{p}-\mathbf{p}'}{\Lambda}\right]^2}\;.\end{aligned} \tag{A2}$$

To see the equivalence of this expression with Eq. (3.9) we need to rewrite Eq. (3.11). By partial integration

$$\begin{aligned}b&=\frac{1}{\beta}\frac{16\pi}{h^3}\int dp\frac{p^3}{3}\left[\frac{\partial n}{\partial p}\ln\frac{n}{1-n}\right]\\&=\frac{16\pi}{h^3}\int dp\frac{p^3}{3}\frac{\partial n}{\partial p}[\mu-\epsilon(p)]\\&=-\mu\rho+\frac{16\pi}{h^3}\int dp\,np^2\epsilon(p)+\frac{16\pi}{h^3}\int dp\frac{p^3}{3}\frac{\partial\epsilon(p)}{\partial p}n\;.\end{aligned} \tag{A3}$$

Combining this with Eqs. (3.10) and (3.12), Eq. (3.9) becomes the same as Eq. (A2).

### 2. Nonequilibrium Pressure

To compute pressure from Eq. (3.6) in the nonequilibrium situation considered in Sec. III, we first note that $f$ in this case is

$$f=\frac{4}{h^3}\theta(p_F-|\mathbf{p}-p_0\hat{z}|)+\frac{4}{h^3}\theta(p_F-|\mathbf{p}+p_0\hat{z}|) \tag{A4}$$

with $(16\pi/3h^3)p_F^3=\rho/2$. The first term in the right-hand side refers to a Fermi sphere centered around $p_0\hat{z}$ and the second to a Fermi sphere around $-p_0\hat{z}$. The values of $p_0$ were chosen for laboratory beam energies 400 and 800 MeV/nucleon, respectively. Here we will restrict ourselves to the momentum-dependent part of MDYI only; momentum-independent parts are easy to take care of. Consider a nucleon in the first Fermi sphere. Define $\mathbf{q}=\mathbf{p}-p_0\hat{z}$; then the appropriate potential consists of two parts: $R^{(1)}+R^{(2)}$ with

$$R^{(1)}=\frac{2C}{\rho_0}\frac{4}{h^3}\int_0^{p_F}d^3\mathbf{q}'\frac{1}{1+\left[\frac{\mathbf{q}-\mathbf{q}'}{\Lambda}\right]^2}\;, \tag{A5}$$

$$R^{(2)}=\frac{2C}{\rho_0}\frac{4}{h^3}\int_0^{p_F}d^3\mathbf{q}'\frac{1}{1+\left[\frac{\mathbf{q}+2\mathbf{p}_0-\mathbf{q}'}{\Lambda}\right]^2}\;. \tag{A6}$$

The integrals appearing in Eqs. (A5) and (A6) can be evaluated in closed form [see Eq. (5.7) in Ref. 4]. $R^{(1)}$ and $R^{(2)}$ for nucleons in the second Fermi sphere can be similarly written down. The integral in Eq. (3.6) involving the derivative of the potential can now be numerically evaluated. The expression for $V$ in Eq. (3.6) is also straightforward in this specific case.

It is possible to rewrite Eq. (3.6) to make the numerics somewhat simpler. Consider the term

$$\begin{aligned}\int d^3p\,p_if\nabla_p^jU&=\int d^3p(\mathbf{p}\cdot\hat{i})f\hat{j}\cdot\nabla_pU\\&=\int d^3p\nabla_p[(\mathbf{p}\cdot\hat{i})f\hat{j}U\\&\qquad-\int d^3pU\nabla_p(\hat{j}f\mathbf{p}\cdot\hat{i})]\;.\end{aligned} \tag{A7}$$

By divergence theorem the first term vanishes and the second term gives $-\int d^3pUp_i(\partial f/\partial p_j)$ and $-\delta_{ij}\int d^3pUf$ (this will be canceled by one of the remaining terms in the pressure tensor). The quantity $(\partial f/\partial p_j)$ for the distribution function here [see Eq. (A4)] gives a $\delta$-function leading to an easy integration.

---

[*] Present address: Physics Deparment, Rutgers University, New Brunswick, NJ 08903.

[1] P. Danielewicz and G. Odyniec, Phys. Lett. **157B**, 146 (1985).

[2] K. G. R. Doss *et al.*, **57**, 302 (1986).

[3] H. A. Gustafsson *et al.*, **52**, 1590 (1984).

[4] G. Welke, M. Prakash, T. T. S. Kuo, S. Das Gupta, and C. Gale, Phys. Rev. C **38**, 2101 (1988).

[5] G. F. Bertsch and S. Das Gupta, Phys. Rep. **160**, 189 (1988); and references therein.

[6] G. F. Bertsch and H. Kruse, and S. Das Gupta, Phys. Rev. C **29**, 673 (1984).

[7] C. Gale, G. F. Bertsch, and S. Das Gupta, Phys. Rev. C **35**, 1666 (1987).

[8] B. Schürmann and W. Zwermann, Phys. Lett. **158B**, 3660 (1985).

[9] J. Aichelin, A. Rosenhauer, G. Peilert, H. Stöcker, and W. Greiner, Phys. Rev. Lett. **58**, 1926 (1987).

[10] R. B. Wiringa, Phys. Rev. C **38**, 2967 (1988).

[11] G. F. Bertsch (private communication).

[12] P. Danielewicz *et al.*, Phys. Rev. C **38**, 120 (1988).

[13] M. Gyulassy, K. A. Frankel, and H. Stöcker, Phys. Lett. **110B**, 185 (1982).

[14] B. ter Haar and R. Malfliet, Phys. Rep. **149**, 207 (1987).

[15] A. Lejeune, J. Cugnon, and P. Grangé, Phys. Rev. C **35**, 861 (1987).

[16] G. F. Bertsch, G. E. Brown, V. Koch, and B. A. Li, Nucl. Phys. **A490**, 745 (1988).

[17] V. R. Pandharipande (private communication).